REPORT DOCUMENTATION PAGE

Form Approved OMB NO. 0704-0188

1. REPORT DATE (DD-MM-YYYY)	2. REPORT TYPE	3. DATES COVERED (From - To)
	New Reprint	-

4. TITLE AND SUBTITLE
Synthesis of nano-scale fast ion conducting cubic Li

5a. CONTRACT NUMBER
W911NF-13-1-0475

5b. GRANT NUMBER

5c. PROGRAM ELEMENT NUMBER

6. AUTHORS
Jeff Sakamoto, Ezhiylmurugan Rangasamy, Hyunjoung Kim, Yunsung Kim, Jeff Wolfenstine

5d. PROJECT NUMBER

5e. TASK NUMBER

5f. WORK UNIT NUMBER

7. PERFORMING ORGANIZATION NAMES AND ADDRESSES
Michigan State University
426 Auditorium Road
Hannah Administration Building, RM 2
East Lansing, MI 48824 -2601

8. PERFORMING ORGANIZATION REPORT NUMBER

9. SPONSORING/MONITORING AGENCY NAME(S) AND ADDRESS (ES)
U.S. Army Research Office
P.O. Box 12211
Research Triangle Park, NC 27709-2211

10. SPONSOR/MONITOR'S ACRONYM(S)
ARO

11. SPONSOR/MONITOR'S REPORT NUMBER(S)
64834-CH.2

12. DISTRIBUTION AVAILIBILITY STATEMENT
Approved for public release; distribution is unlimited.

13. SUPPLEMENTARY NOTES
The views, opinions and/or findings contained in this report are those of the author(s) and should not contrued as an official Department of the Army position, policy or decision, unless so designated by other documentation.

14. ABSTRACT
A solution-based process was investigated for synthesizing cubic Li7La3Zr2O12 (LLZO), which is known to exhibit the unprecedented combination of fast ionic conductivity, and stability in air and against Li. Sol–gel chemistry was developed to prepare solid metal–oxide networks consisting of 10 nm cross-links that formed the cubic LLZO phase at 600 degrees C. Sol–gel LLZO powders were sintered into 96% dense pellets using an induction hot press that applied pressure while heating. After sintering, the average LLZO grain size was 260 nm,

15. SUBJECT TERMS
batteries, solution based process, synthesizing cubic LLZO, fast ionic conductivity

16. SECURITY CLASSIFICATION OF:			17. LIMITATION OF ABSTRACT	15. NUMBER OF PAGES	19a. NAME OF RESPONSIBLE PERSON
a. REPORT	b. ABSTRACT	c. THIS PAGE			Jeff Sakamoto
UU	UU	UU	UU		19b. TELEPHONE NUMBER 517-432-7393

Report Title

Synthesis of nano-scale fast ion conducting cubic Li

ABSTRACT

A solution-based process was investigated for synthesizing cubic Li7La3Zr2O12 (LLZO), which is known to exhibit the unprecedented combination of fast ionic conductivity, and stability in air and against Li. Sol–gel chemistry was developed to prepare solid metal–oxide networks consisting of 10 nm cross-links that formed the cubic LLZO phase at 600 degrees C. Sol–gel LLZO powders were sintered into 96% dense pellets using an induction hot press that applied pressure while heating. After sintering, the average LLZO grain size was 260 nm, which is 13 times smaller compared to LLZO prepared using a solid-state technique. The total ionic conductivity was 0:4 mS cm1 at 298 K, which is the same as solid-state synthesized LLZO. Interestingly, despite the same room temperature conductivity, the sol–gel LLZO total activation energy is 0.41 eV, which 1.6 times higher than that observed in solid-state LLZO (0.26 eV). We believe the nano-scale grain boundaries give rise to unique transport phenomena that are more sensitive to temperature when compared to the conventional solid-state LLZO.

REPORT DOCUMENTATION PAGE (SF298)
(Continuation Sheet)

Continuation for Block 13

ARO Report Number 64834.2-CH
Synthesis of nano-scale fast ion conducting cub...

Block 13: Supplementary Note

Approved for public release; distribution is unlimited.

Nanotechnology **24** (2013) 424005 (8pp) doi:10.1088/0957-4484/24/42/424005

Synthesis of nano-scale fast ion conducting cubic $Li_7La_3Zr_2O_{12}$

Jeff Sakamoto[1], Ezhiylmurugan Rangasamy[1], Hyunjoung Kim[1], Yunsung Kim[1] and Jeff Wolfenstine[2]

[1] Department of Chemical Engineering and Materials Science, Michigan State University, 2527 Engineering, East Lansing, MI 48824, USA
[2] Army Research Laboratory, RDRL-SED-C, 2800 Powder Mill Road, Adelphi, MD 20783, USA

E-mail: jsakamot@msu.edu

Received 31 January 2013, in final form 2 April 2013
Published 25 September 2013
Online at stacks.iop.org/Nano/24/424005

Abstract
A solution-based process was investigated for synthesizing cubic $Li_7La_3Zr_2O_{12}$ (LLZO), which is known to exhibit the unprecedented combination of fast ionic conductivity, and stability in air and against Li. Sol–gel chemistry was developed to prepare solid metal–oxide networks consisting of 10 nm cross-links that formed the cubic LLZO phase at 600 °C. Sol–gel LLZO powders were sintered into 96% dense pellets using an induction hot press that applied pressure while heating. After sintering, the average LLZO grain size was 260 nm, which is 13 times smaller compared to LLZO prepared using a solid-state technique. The total ionic conductivity was 0.4 mS cm^{-1} at 298 K, which is the same as solid-state synthesized LLZO. Interestingly, despite the same room temperature conductivity, the sol–gel LLZO total activation energy is 0.41 eV, which 1.6 times higher than that observed in solid-state LLZO (0.26 eV). We believe the nano-scale grain boundaries give rise to unique transport phenomena that are more sensitive to temperature when compared to the conventional solid-state LLZO.

1. Introduction

Keeping up with the demands for vehicle electrification requires a revolutionary change in electrochemical energy storage [1–3]. Li–S, Li-air, solid-state, and high-voltage Li-ion batteries are potential candidates to meet the demands; however new electrolytes are required to enable these technologies [2, 4]. Specifically, solid ceramic electrolytes are a promising class of materials to enable new battery chemistries [5]. Ideally, the ceramic electrolyte should have the following properties: (i) fast ion conductivity with a transference number of 1, (ii) non-flammable, (iii) stable in air and over a wide electrochemical potential range, and (iv) relatively simple to synthesize in powder form for subsequent sintering into a dense membrane or integration into a polymer composite membrane [6]. Numerous solid-state oxide Li-ion conductors have been investigated, such as LiSICON, perovskites and garnets [5, 7, 8]. Of these the cubic garnet with a nominal composition of $Li_7La_3Zr_2O_{12}$ (LLZO) has one of the highest ionic conductivities ($>10^{-4}$ S cm^{-1}) [9, 10] and is believed to be stable against metallic Li [11].

Recent work has involved the solid-state synthesis of LLZO [9–14]. Solid-state synthetic techniques are facile and convenient for investigating new materials in a laboratory setting where relatively small (10 g) sample batches are required. However, to commercialize LLZO, flexible, scalable and low-cost synthetic techniques are required. Solid-state synthesis typically does not offer the flexibility to make nano-dimensional particles with high sinterability nor the ability to coat/protect electrode powders. By developing a solution-based process to synthesize LLZO, the fabrication of several battery components/designs can be improved or enabled (figure 1). First, Li–S, Li-air, solid-state or other Li-metal anode battery configurations require a solid electrolyte membrane that is electrochemically, and mechanically stable against Li (figure 1(a)). To prevent the catholyte from reacting with Li and to suppress Li dendrite penetration, the membrane must be dense. Typically, the LLZO is prepared using a solid-state technique that produces micron-scale grains that must be sintered at >1150 °C [14] to eliminate interconnected porosity. One problem with conventional high-temperature synthesis is Li loss. Thus,

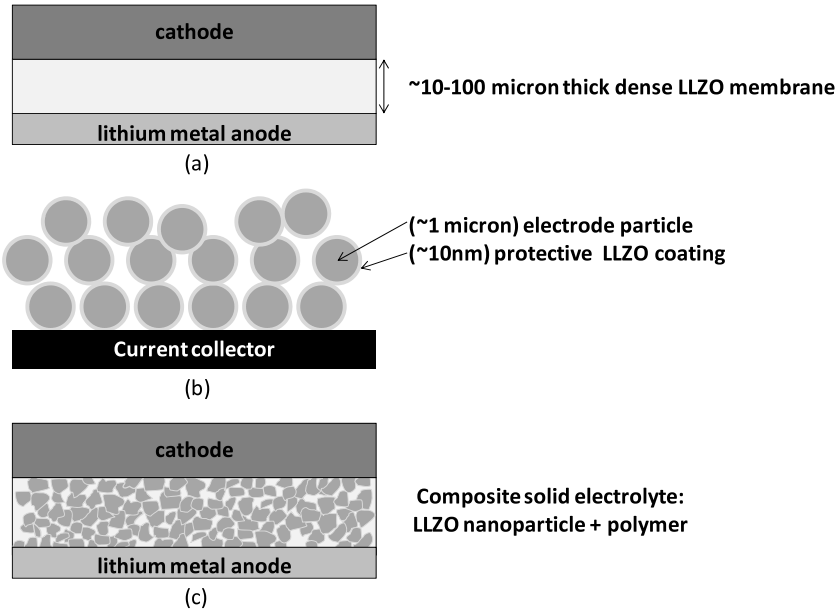

Figure 1. The ceramic electrolyte $Li_7La_3Zr_2O_{12}$ (LLZO) may enable numerous new battery components, such as: (a) membranes for use in Li–sulfur, Li-air or solid-state batteries, (b) a high-voltage protective coating to enable high-voltage cathodes, and (c) an ionically conductive additive to suppress Li dendrites in polymer electrolyte membranes.

means to reduce the sintering temperature are needed. One possible approach is to use small particles, such as nano-scale particles, that can be sintered at lower temperatures compared to powders prepared through the conventional solid-state process [15]. Second, there is significant interest in integrating high-voltage cathodes into Li-ion batteries [16]. However, the lack of electrolytes that are stable at high voltage hinders their widespread implementation. Likewise, developing a sol–gel approach for coating high-voltage cathodes could enable their use (figure 1(b)). Third, an alternative approach for fabricating solid-state batteries could involve LLZO powder/solid polymer electrolytes (figure 1(c)) [6]. In this approach, the purpose of the polymer electrolyte is to enable low-temperature fabrication (compared to the approach shown in figure 1(a)) while the purpose of the LLZO powders is to act as a stiff matrix to suppress Li dendrite penetration. By developing a sol–gel process, the LLZO particle size can be precisely tuned, from the nanometer to the micron scale, to form a percolative, sufficiently stiff [17], and tortuous network to block Li dendrite penetration while maintaining high ionic conductivity in polymer/particle composite electrolytes.

In this work, a sol–gel technique capable of synthesizing LLZO is described. A Zr-alkoxide is combined with soluble Li, La, and Al cations capable of hydrolyzing and condensing into a continuous solid network forming a metal–oxide network at room temperature. We believe the ability to control the poly-condensation of multiple cationic species into an oxide network is unique to this sol–gel process. In addition to the envisioned uses described in figure 1, the ability to form a metal–oxide network at room temperature could also allow calcination (phase formation) in an inert atmosphere. Thus, the ability to integrate LLZO into composite anodes with materials that are highly air sensitive, such as nanoSi, could be enabled.

Below, the new sol–gel process is described for synthesizing cubic LLZO. To analyze the native LLZO network, supercritical fluid extraction was used to preserve the nano-scale features and allow for vibrational spectroscopy to characterize the types of bonding. X-ray diffraction data as a function of calcination temperature is reported to evaluate the phase formation. Lastly, the sol–gel powders were sintered, using uniaxial hot pressing, to prepare dense specimens for electrochemical impedance spectroscopy.

2. Experimental details

2.1. Sol–gel synthesis

$LiNO_3 \cdot xH_2O$ ($x = 0.5$, 99.999% Alfa Aesar), $La(NO_3)_3 \cdot 6H_2O$ (99.9% Alfa Aesar), and $Zr(OH_7C_3)$ (70% w/w in n-propanol, Alfa Aesar) were used as the gel precursors.

1-propanol (ACS 99.5% Alfa Aesar) was used as the diluting solvent and acetic acid (Glacial ACS 99.7% Alfa Aesar) was used as a chelating agent. 0.24 moles of aluminum was added using aluminum oxide (50 nm, Merck) to the precursor solution before gelation occurs. The process flow diagram, along with the precursor compositions, is shown in figure 2. The precursors were separately dissolved in *n*-propanol. The precursor solutions were then mixed along with the addition of aluminum oxide powders. Gelation occurred in approximately 30 min, which was followed by 24 h of ageing to assure the reaction was complete. The gels were subsequently ambient dried for 48 h followed by heat treatment at 450 °C in air to remove organics. The dried powder was cold pressed into 0.5″ diameter pellets using a stainless steel die at 40 MPa. The cold pressed samples were calcined in air at 600, 800, 900 and 1000 °C in air for 4 h using a heating rate of 100 °C h^{-1} (Thermo Scientific Lindberg Blue M Mini-Mite).

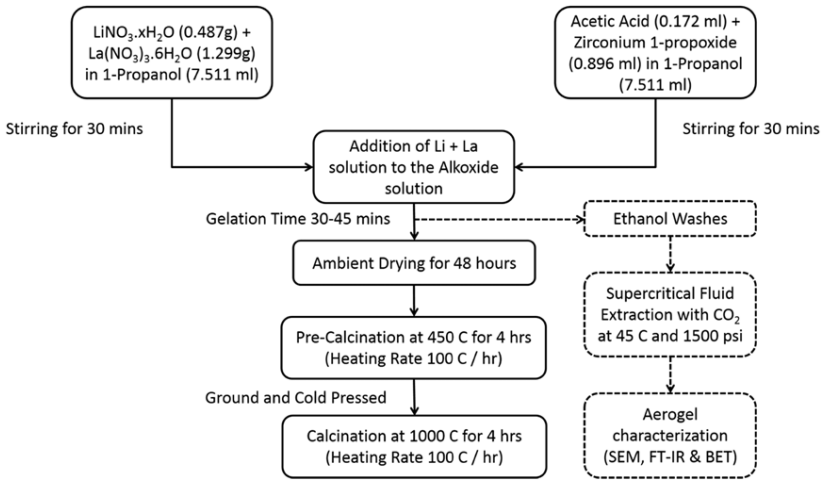

Figure 2. Process flow diagram describing the sol–gel synthesis of $Li_7La_3Zr_2O_{12}$ gels. The hatched section of the flow diagram indicates that the supercritical process was only used to characterize the native gel network before the porosity is collapsed during drying.

Zirconia-coated crucibles were used for calcination. The sample powders were analyzed using x-ray powder diffraction (Bruker AXS D8 Advance with Da Vinci) for identification of crystal phases. To determine the concentration of cations, inductively coupled plasma (ICP) chemical analysis was conducted by Galbraith Laboratories (Tennessee, USA), which was the same procedure used in previous work [10].

2.2. Supercritical drying

To prepare for supercritical drying, wet gels were washed with pure ethanol. Three ethanol washes were used, where each wash was at least 10 times the volume of the gel, and the gels were submerged for 24 h each wash. Following the ethanol washing, the gels were placed in a 1 liter critical point dryer (Pressure Products Inc). The ethanol within the gel pores was exchanged with ultra-high purity liquid carbon dioxide (Airgas). Once the ethanol was replaced by liquid carbon dioxide, the temperature and pressure were raised to 45 °C and 10 MPa, respectively, to establish supercritical conditions. The temperature was maintained at 45 °C while the pressure was decreased to ambient conditions. Supercritically dried gels were then stored in a 0.5 ppm moisture, 0.2 ppm oxygen, argon-filled glovebox until further testing. This was done to prevent reactions with moisture in ambient air that could affect the nitrogen sorption measurements. Brunauer–Emmett–Teller (BET) surface area and pore volume characterization was performed by nitrogen adsorption (Micromeritics ASAP 2020). Ultra-high-purity helium and ultra-high-purity nitrogen were used to measure free space and surface area, respectively. Samples were degassed under vacuum at 80 °C for twelve hours to remove residual water vapor before nitrogen adsorption was initialized.

2.3. Material and electrochemical characterization

Supercritically dried sol–gel samples were cut into approximately 1 mm^3 cubes and osmium coated for imaging. Scanning electron microscopy (SEM) images were obtained with a field emission JEOL 7500F electron microscope. Grain sizes on SEM fractographs were calculated using linear intercept analysis. Briefly, lines of known length were drawn on the SEM fractographs. The number of grains were counted per line. The line length was divided by the number of grains intersected by the line to obtain the average grain size.

Thermogravimetric/differential scanning calorimetry (TG/DSC) was performed on sol–gel synthesized LLZO. To reduce the mass loss contribution for solvents and other organic compounds, the gels were pre-heated at 450 °C in air for 4 h before performing TG/DSC analysis. A Netzsch STA 449 TG/DSC analyzer was used under flowing air.

After calcination, the powders were hot pressed at 1000 °C under 40 MPa pressure for 1 h under flowing argon. The pellet density was determined by measuring the weight and geometric volume of a parallelepiped. Li-ion conductivity was determined using AC electrochemical impedance spectroscopy (EIS) with a VersaSTAT4 potentiostat over a frequency range of 10 Hz–800 kHz and potential amplitude of 100 mV. The Arrhenius measurements were made using a load frame to apply 340 kPa pressure while heating. The 12.7 mm diameter electrode pins that made contact with the specimen were instrumented with 0.5 mm diameter. Type K thermocouples to measure the temperature. For electrochemical measurements, the sintered pellets were coated with Au films of an approximate thickness of 105 nm using sputter coating. A load frame applied a constant 0.34 MPa pressure during EIS measurements. Arrhenius measurements were conducted by placing the specimen and assembly into an oven. Type K thermocouples were inserted into each of the 12.7 mm diameter metal electrode pins that applied pressure against the specimen. The temperature was varied between room temperature and 70 °C.

3. Results and discussion

3.1. Gel characterization

Typical sol–gel systems require a controlled change in pH to enable poly-condensation after hydrolysis of the

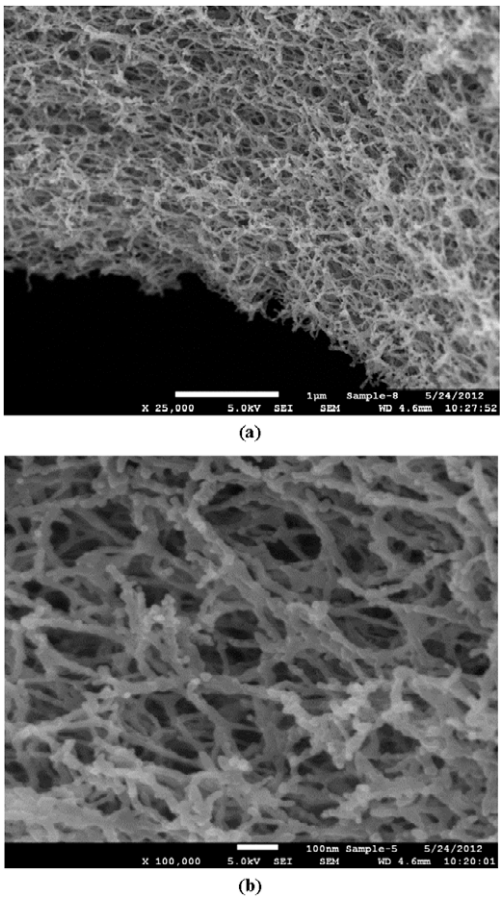

Figure 3. High-resolution scanning electron microscopic analysis of supercritically dried $Li_7La_3Zr_2O_{12}$ gel: (a) 25 000 and (b) 100 000×.

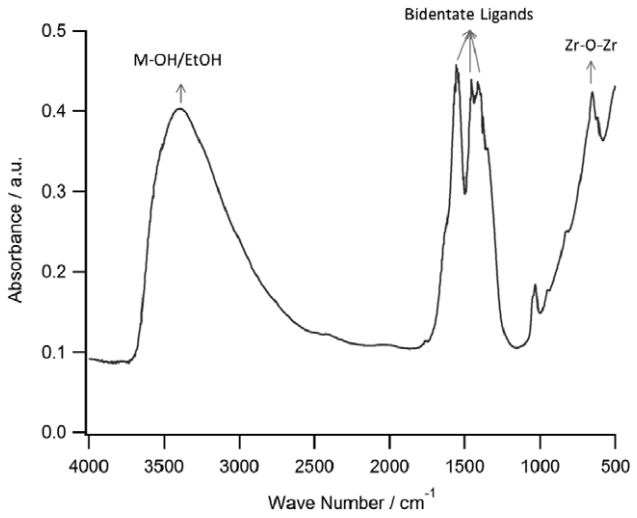

Figure 4. Fourier transform infrared spectra of supercritically dried $Li_7La_3Zr_2O_{12}$ gel.

alkoxide precursor [18, 19]. However, owing to the high reactivity of Zr-alkoxides, spontaneous hydrolyzation and poly-condensation can occur in the parent solvent even in the absence of pH change [20]. In some cases this reaction has been found to be so rapid that precipitation results [21]. Because of the multiple cationic species that comprise LLZO, a method for slowing or controlling the condensation rate of the Zr-alkoxide was necessary to achieve uniform gelation. In this work, acetic acid was added as a chelating agent to slow down the hydrolysis and to control the poly-condensation reaction of Zr in the Li–La–Zr–Al containing sol (figure 2). Two separate cation solutions were prepared. One solution contained Li and La cations with 50 nm aluminum oxide particles in suspension. Aluminum (from the aluminum oxide) is necessary to stabilize the cubic phase [10, 12], and was added in solid rather than solution form to simplify the sol–gel chemistry. The second solution contained the zirconium alkoxide chelated by acetic acid. The two solutions were stirred separately for 30 min before combination. After combination, the mixture or Li, La, Zr, alumina gelled to form rigid transparent gels.

To evaluate the gel in its native or as-gelled state, supercritical fluid extraction was conducted to analyze the solid network and pore morphology. SEM images of the supercritically dried sol–gel (aerogel) (figure 3) illustrate the highly interconnected solid network consisting of cross-links approximately ten nanometers wide. BET analysis of the dried gel revealed a high surface area (292 m^2 g^{-1}) with a large fraction of microporosity (33%). In order to confirm the presence of Zr–O–Zr bonding, the supercritically dried gel was characterized using Fourier transform infrared (FT–IR) spectroscopy. The FT–IR spectrum (figure 4) indicates absorbance peaks at 666 cm^{-1}, characteristic of Zr–O–Zr bonds, as has been observed in other zirconia gels [22–24]. These studies also indicate the absorbance peaks observed between 1300 and 1700 cm^{-1} are characteristic of the bidentate ligands, confirming the presence of CH_3COO^- within the structure [20]. There are other absorbance peaks at approximately 1000 and 800 cm^{-1}, however, that could not be clearly identified at this time. Nevertheless, the FT–IR spectrum confirms the presence of Zr–O–Zr bonds; a feature we believe is unique to the sol–gel process.

The supercritical fluid extraction process describe above preserved the gel's native morphology and chemistry in the dry state as if it were wet. This enabled high-resolution SEM, BET, and FT–IR analysis of the gel network. However, as observed by other groups, solution-based approaches for synthesizing LLZO require heating to obtain the cubic garnet crystal structure [25, 26]. Thus, x-ray diffraction analysis as a function of calcination temperature is presented and discussed in the next subsection.

3.2. Effect of calcination temperature

The previous subsection characterized sol–gel derived LLZO in the supercritically dried state; a form that is useful for preserving morphology, but not representative of a material dried by practical means. Conventional drying, such as heating or calcination in air, is a more practical method for drying gels. This subsection characterizes the effect of calcination temperature on gels that were pre-heated to 450 °C in air for 4 h, which was sufficient to drive off solvents and organics. LLZO, with the space group

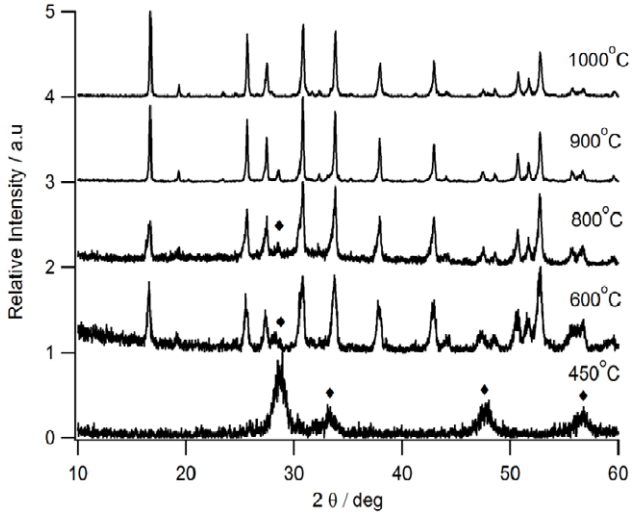

Figure 5. X-ray diffraction analysis of sol–gel synthesized $Li_7La_3Zr_2O_{12}$ powders. The bottom spectrum (450 °C) indicates the presence of semi-crystalline $La_2Zr_2O_7$ (pyrochlore, highlighted by symbol ♦). All other spectra were obtained from calcining at the indicated temperature, in addition to heating to 450 °C for 4 h. Cubic LLZO (garnet) is the primary phase present when heating to 600 °C or higher.

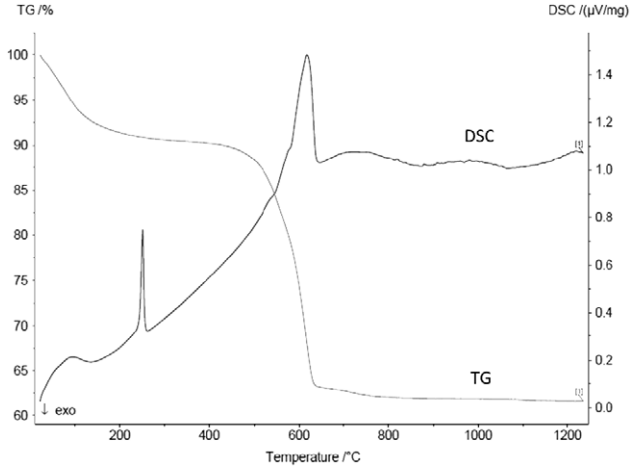

Figure 6. Thermogravimetric/differential scanning calorimetric (TG/DSC) curves for sol–gel synthesized $Li_7La_3Zr_2O_{12}$ powder.

$Ia\bar{3}d$, is the desired crystallographic form known to exhibit 0.4 mS cm^{-1} conductivity at room temperature [9–11]. Likewise, confirming the presence of this phase was assessed using x-ray diffraction as a function of calcination temperature in air.

The x-ray diffraction data as function of calcination temperature are shown in figure 5. After heating at 450 °C in air for 4 h, nanocrystalline $La_2Zr_2O_7$ (pyrochlore) is present. According to the Scherrer equation [27], the crystallite size of the pyrochlore phase is 10 nm. It is also important to note that, in general, at the lower temperature where the pyrochlore is the only crystallographic phase detected, there is significant noise in the spectra [25, 26]. It is believed that the noise is a result of attenuation from a significant volume fraction of an amorphous Li-containing phases, i.e. unreacted Li. When the LLZO gel is calcined at 600 °C or above, the desired cubic LLZO (garnet) phase is formed. After calcining at 600 and 800 °C, there are still trace amounts of $La_2Zr_2O_7$, but after calcining at 900 and 1000 °C only cubic LLZO is present.

From the above x-ray diffraction data, several observations can be made. First, the reaction pathway for the sol–gel LLZO in this work is similar to that observed in the Pechini [25] and citrate-nitrate method [26], in that $La_2Zr_2O_7$ is the first crystallographic phase formed upon heating. In this work, however, the $La_2Zr_2O_7$ reacts with Li to form cubic LLZO at 600 °C, whereas the same reaction occurred at 650 and 700 °C for the Pechini [25] and citrate-nitrate method [26], respectively. Secondly, the LLZO that was synthesized with the Pechini method was not stable at 1000 °C and transformed into tetragonal LLZO (garnet), which is the minimum temperature to achieve a reasonable density. Because Al was not present in the LLZO prepared using the Pechini method, the LLZO transformed into tetragonal LLZO above 800 °C. In this work, we added 0.24 moles of Al to stabilize cubic LLZO upon formation (600 °C) up to 1000 °C (the sintering temperature). The absence of peak doublets [10] in figure 5 confirms the presence of cubic LLZO up to 1000 °C. Thirdly, because poly-condensation occurs, the sol–gel derived materials consist of M–O bonding after gelation, thus calcination can be conducted entirely in an inert atmosphere to form the cubic garnet phase (x-ray diffraction analysis confirmed this, but the data is not shown for gels that were heated from the as-gelled state to 1000 °C in argon). This is in contrast to the Pechini and citrate-nitrate methods, which may require heating in air to provide oxygen to form cubic LLZO. Perhaps the most obvious advantage of this process can be envisioned in figure 1(b). Because cubic LLZO can be synthesized through the liquid state and calcined in an inert atmosphere, air sensitive electrodes, such as nanosilicon, can be coated by this process. The LLZO coating could be relatively thin, and protect the nanosilicon from excessive solid electrolyte interphase formation, thus improving the performance.

The TG/DSC analysis in air of sol–gel LLZO is shown in figure 6. The powder was pre-heated to 450 °C for 4 h in air to dry the sample (before TGA/DSC analysis), as was the case above. First, an endothermic peak occurs at approximately 250 °C. Because there is no coinciding weight loss and $La_2Zr_2O_7$ does not go through a phase change below 800 °C, the origin of the peak at 250 °C is not known at this time. Above approximately 500 °C, significant weight loss occurs up to approximately 650 °C. Coinciding with the significant weight loss, the onset of a significant endothermic peak is observed at approximately 600 °C. The endothermic peak is believed to represent the formation of cubic LLZO, which agrees with the x-ray diffraction analysis above. Above 650 °C, little weight change and no significant endo/exothermic peaks are observed, indicating the cubic LLZO phase is stable once formed. Additionally, inductively coupled plasma (ICP) chemical analysis confirmed the concentration of cations was in good agreement with the intended formulation. ICP determined that the cation formulation was Li = 6.28, La = 3.0, Zr = 2.0

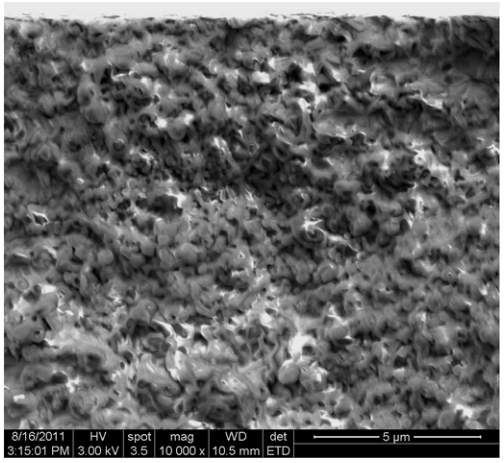

Figure 7. A scanning electron image of an intentionally fractured sol–gel $Li_7La_3Zr_2O_{12}$ hot pressed specimen.

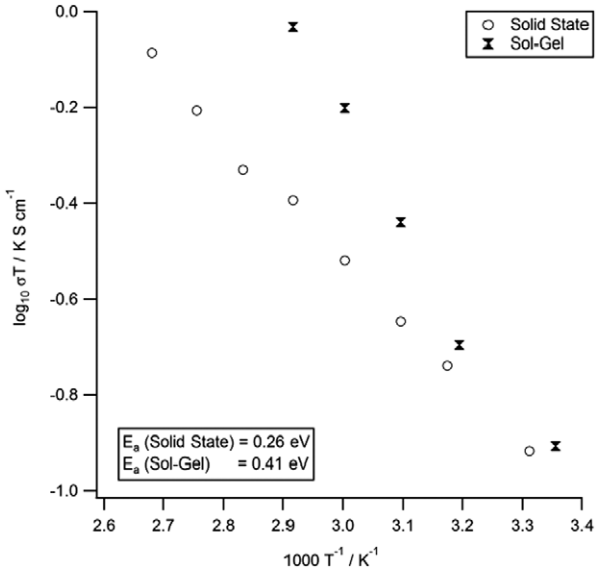

Figure 8. Arrhenius analysis of sol–gel synthesized, hot pressed $Li_7La_3Zr_2O_{12}$.

and Al = 0.24. This is also in close agreement to what was intended, and similar in composition to the material prepared using solid-state synthesis [10].

3.3. Sintering and electrochemical impedance characterization

If the desired battery component is a dense membrane 90% minimum with closed porosity [28] (figure 1(a)), sintering to achieve high density is necessary. In this work, sol–gel synthesized LLZO powders were hot pressed at 1000 °C under 40 MPa. A fracture surface of the hot pressed sol–gel LLZO specimen is shown in figure 7. Relatively little porosity was observed, which agrees with the geometric density measurement of 96% relative density. Additionally, the average grain size was 260 nm. Compared to solid-state synthesized cubic LLZO powders (solid-state LLZO), with an average grain size of 3.3 μm after hot pressing [10], the sol–gel LLZO grains were 13 times smaller. Additionally, fracture in the sol–gel LLZO was primarily intergranular, compared to mixed inter- and intragranular observed in the solid-state LLZO sintered under the same conditions [10]. The ability to control the particle size down to the hundreds of nanometer scale or less could enable tuning to achieve optimum conductivity and mechanical properties. It is known that the grain size and fracture strength are inversely related, i.e. the smaller the grain size the higher the fracture strength [15, 28]. A ceramic electrolyte membrane should be in the 10–100 μm thick range if it is to be considered practical for solid-state, Li–S or Li-air batteries [4], thus the fracture strength must be adequate to enable fabrication and handling. By using sol–gel synthesized powders, the grain size can be significantly reduced, compared to the solid-state synthesized powder, to increase fracture strength and facilitate the development of LLZO ceramic electrolyte membrane technology.

Figure 8 shows the Arrhenius plot of the total Li-ion conductivity of the sol–gel synthesized LLZO as a function of temperature. For comparison, solid-state LLZO data from previous work (which has a similar Al and Li content as mentioned above) is also included [10]. The activation energy was estimated from the slope of the line in the temperature range 25–70 °C. From figure 8, several important points can be made. Firstly, at room temperature the total conductivities for the sol–gel and solid-state LLZO are nearly the same, ~0.4 mS cm^{-1}. Secondly, as temperature increases the total conductivity for the sol–gel material is higher than that for the solid-state material. Thirdly, the activation energy for the sol–gel LLZO material is higher (0.41 eV) compared to the solid-state LLZO material (0.26 eV).

It is known that the total conductivity is a function of the lattice conductivity and the grain boundary component. Since the Al and Li content are the same it would be expected that the lattice conductivity for both sol–gel and solid-state materials should be same, in which case the difference in total conductivity is due to the difference in the conductivity of the grain boundary component for each material. In general the conductivity of the grain boundary component is influenced by the density, grain size and chemistry at the grain boundaries [29, 30]. Both of these materials have roughly the same density, thus, any difference in density is not likely the cause for the difference in conductivity shown in figure 8. It is known, for grain sizes in the micron region, that as the grain size increases the grain boundary conductivity increases [31, 32]. Thus, one expects in a first approximation that the solid-state LLZO material with larger grain size (5 μm) compared to the sol–gel LLZO material (260 nm) would have a higher grain boundary conductivity and, hence, a higher total conductivity. However the opposite trend is observed in figure 8. It has been shown for $LiNbO_3$ [33], $Li_4Ti_5O_{12}$ [34], ZrO_2 [35], CeO_2 [36] and TiO_2 [37] that as the grain size changed from the micron to nanometer scale that the total conductivity of the nanocrystalline material was higher than that for the microcrystalline material, in agreement with results of this study. In general the lattice

conductivities of the nanocrystalline and microcrystalline materials were similar, suggesting that the higher total conductivity of the nanocrystalline materials was associated with higher grain boundary conductivity in the nanocrystalline material compared to the microcrystalline material [34, 36, 37]. It was suggested that in the nanocrystalline material, because of its larger grain boundary area, that this resulted in a lower impurity segregation (impurities act to block Li-ion conduction) on the grain boundaries, leading to higher conductivity grain boundaries compared to grain boundaries in the microcrystalline material [36–38]. It is likely that a similar phenomenon occurs for the case of nanocrystalline versus microcrystalline LLZO. To confirm this would require detailed electron microscopy examination of grain boundaries for the two grain size materials.

It would be expected because the total conductivity of the nanocrystalline material is higher than for microcrystalline material that in a first approximation the activation for total conductivity for the nanocrystalline material be would equal to or lower that for the microcrystalline material if the grain boundaries are free of impurities. However the activation energy for the nanocrystalline material is about 1.6× times that for the microcrystalline material. Reasons for this discrepancy are not apparent. One possible reason could be a difference in the impurities at the boundaries, since these were made with different starting materials and involved different processing steps. Another possible reason could be that even though the Al and Li content are the same there could be a difference in purity which could affect not only grain boundary but also lattice conductivity. In order to investigate these possible reasons a detailed characterization of the chemistry of grain interiors and grain boundaries is required.

In any case it has been shown that the total conductivity of sol–gel synthesized LLZO is equal to that of solid-state LLZO at room temperature, and becomes higher as the temperature is increased. Consequently, because the fracture strength scales with decreasing grain size, sol–gel synthesized LLZO offers conductivity and strength advantages compared to solid-state synthesized LLZO.

4. Conclusions

A novel sol–gel process was investigated to enable the synthesis of a nano-scale fast ion conducting ceramic electrolyte technology based on cubic $Li_7La_3Zr_2O_{12}$ (LLZO) with the garnet structure. The sol–gel chemistry was tailored to synthesize a solid metal–oxide gel network at room temperature, allowing calcination in inert atmospheres. Supercritical fluid extraction preserved the gel network in the as-gelled state, allowing the detailed morphological and chemical analysis. The as-gelled metal–oxide network consisted of an interconnected network of approximately 10 nm wide cross-links. Forming the preferred cubic LLZO phase required heating to a minimum temperature of 600 °C, above which no phase transitions occurred up to 1000 °C. Sintering the sol–gel powders was achieved using a novel induction hot press technique that achieved 96% dense specimens with a grain size of 260 nm. Interestingly, despite a 13-fold decrease in grain size, the total conductivity of the sol–gel synthesized material was the same, 0.4 mS cm^{-1} at 25 °C, as the solid-state synthesized material. Furthermore, even though they exhibited the same room temperature conductivity, the sol–gel LLZO activation energy (0.41 eV) was much higher than the solid-state LLZO activation energy (0.26 eV). We believe the nano-scale grain boundaries give rise to unique transport phenomena that are more sensitive to temperature and could create opportunities to further enhance the conductivity of LLZO.

Acknowledgment

JS, EL, HK, and YK would like to acknowledge the support of the US Army Research Office under contract/grant number. W911NF0910451.

References

[1] Bruce P G, Freunberger S A, Hardwick L J and Tarascon J-M 2012 *Nature Mater.* **11** 19
[2] Dunn B, Kamath H and Tarascon J-M 2011 *Science* **334** 928
[3] Tarascon J-M and Armand M 2001 *Nature* **414** 359
[4] Birke P, Salam F, Doring S and Weppner W 1998 *Solid State Ion.* **118** 149
[5] Knauth P 2009 *Solid State Ion.* **180** 911
[6] Sabau A S, Tenhaeff W E, Dudney N J and Claus D 2012 *J. Power Sources* **201** 280
[7] Wakihara M, Minami T, Tatsumisago M, Iwakura C, Kohjiya S and Tanaka I 2005 *Solid State Ionics for Batteries* (Berlin: Springer)
[8] Stramare S, Thangadurai V and Weppner W 2003 *Chem. Mater.* **15** 3974
[9] Murugan R, Thangadurai V and Weppner W 2007 *Angew. Chem.* **46** 7778
[10] Rangasamy E, Wolfenstine J and Sakamoto J 2012 *Solid State Ion.* **206** 28
[11] Ohta S, Kobayashi T and Asaoka T 2011 *J. Power Sources* **196** 3342
[12] Geiger C A, Alekseev E, Lazic B, Fisch M, Armbruster T, Langner R, Fechtelkord M, Kim N, Pettke T and Weppner 2010 *Inorg. Chem.* **50** 1089
[13] Rangasamy E, Wolfenstine J, Allen J and Sakamoto J 2013 *J. Power Sources* **230** 261
[14] Huang M, Liu T, Deng Y, Geng H, Shen Y, Lin Y and Nan C W 2011 *Solid State Ion.* **204** 41
[15] Chiang Y M, Birnie D and Kingery W D 1996 *Physical Ceramics* (New York: Wiley)
[16] Allen J, Jow T R and Wolfenstine J 2011 *J. Power Sources* **196** 8656
[17] Monroe C and Newman J 2005 *J. Electrochem. Soc.* **152** A396
[18] Livage J, Sanchez C, Henry M and Doeuff S 1989 *Solid State Ion.* **32/33** 633
[19] Livage J 1986 *J. Solid State Chem.* **64** 322
[20] Livage J and Sanchez C 1992 *J. Non-Cryst. Solids* **145** 11
[21] Kundu D and Ganguli D 1986 *J. Mater. Sci. Lett.* **5** 293
[22] Atik M, Kha C and Neto P L 1995 *J. Mater. Sci. Lett.* **14** 178
[23] Wolf C and Rüssel C 1992 *J. Mater. Sci.* **27** 3749
[24] Balamurugan A, Kannan S and Rajeswari S 2003 *Mater. Lett.* **57** 4202
[25] Kokal I, Somer M, Notten P H L and Hintzen H T 2011 *Solid State Ion.* **185** 42
[26] Janani N, Ramakumar S, Dhivya L, Deviannapoorani C, Saranya K and Murugan R 2011 *Ionics* **17** 575

[27] Cullity B D 1978 *Elements of X-Ray Diffraction* (London: Addison-Wesley)
[28] Barsoum M V 1997 *Fundamentals of Ceramics* (New York: McGraw-Hill)
[29] Baurle J E 1969 *J. Phys. Chem. Solids* **30** 2657
[30] Halle S M, West D L and Campbell J 1998 *J. Mater. Res.* **13** 1576
[31] Sutorik A C, Green M D, Cooper C, Wolfenstine J and Gilde G 2012 *J. Mater. Sci.* **47** 6992
[32] Ban C W and Choi G M 2001 *Solid State Ion.* **140** 285
[33] Verkerk M J, Midelhuis B J and Burggraff A J 1982 *Solid State Ion.* **6** 159
[34] Heitjans P, Masoud M, Feldhoff A and Wilkening M 2007 *Faraday Discuss.* **134** 67
[35] Iwanaik W, Fritzsche J, Zukalova M, Winter R, Wilkening M and Heitjans P 2009 *Defect Diffus. Forum* **289–292** 565
[36] Mondal P, Klein A, Jaegermann W and Hahn H 1999 *Solid State Ion.* **118** 331
[37] Chiang Y -M, Lavik E B, Kosacki I and Tuller H L 1997 *J. Electroceram.* **1** 7
[38] Demetry C and Shi X 1999 *Solid State Ion.* **6** 271